Intermetallics 129 (2021) 107029

Contents lists available at ScienceDirect

Intermetallics

journal homepage: http://www.elsevier.com/locate/intermet

Severe warm-rolling mediated microstructure and texture of equiatomic CoCrFeMnNi high entropy alloy: A comparison with cold-rolling

J. Saha, G. Ummethala, S.R.K. Malladi, P.P. Bhattacharjee *

Department of Materials Science and Metallurgical Engineering Indian Institute of Technology, Hyderabad Kandi, Sangareddy, 502285, India

ARTICLE INFO

Keywords:
High entropy alloys
Deformation
Recrystallization
Microstructure
Texture
Properties

ABSTRACT

The effect of severe warm-rolling on the microstructure and texture development in FCC equiatomic CoCrFeMnNi HEA was investigated in the present work. For this purpose, the HEA was warm-rolled to 90% reduction in thickness at 600 °C and annealed for 1 h at temperatures up to 1200 °C. To highlight the effect of warm-rolling, a critical comparison was made with similarly deformed and annealed cold-rolled HEA. The warm-rolled HEA showed an ultrafine lamellar microstructure, which was, however, significantly coarser than the cold-rolled HEA. The significantly coarser microstructure in the warm-rolled HEA could be attributed to the dynamic annihilation of dislocations during deformation. Warm-rolled HEA showed a pure metal or copper type texture instead of a predominantly brass type texture in the cold-rolled HEA. The stark differences in the deformation texture could be attributed to the increase in the SFE at the temperature of warm-rolling, which promoted more homogeneous deformation by dislocation slip over twin mediated deformation and extensive shear band formation. The lower stored energy and coarser deformation structure of the warm-rolled HEA resulted in higher recrystallization temperature, and consistently larger recrystallized grain size than the cold-rolled HEA. Annealing also resulted in the weakening of the recrystallization texture owing to the absence of strong preferential nucleation or growth. The HEA warm-rolled and annealed at 750 °C resulted in a fine-grained, completely recrystallized microstructure with the optimum strength-ductility combination. The present results revealed that warm-rolling could be effectively used as a processing route for tailoring microstructure and properties of CoCrFeMnNi HEA.

1. Introduction

The conventional approach to alloy design hinges on selecting one principal element to which other alloying elements are added to improve the existing properties or even achieve new properties. Although the traditional approach has been remarkably successful in developing a wide range of useful engineering alloys, the scope for creating advanced alloys is squeezed, which necessitates a fresh approach to alloy design. In this context, the advent of high entropy alloys (HEAs) signifies a paradigm shift [1].

HEAs are originally proposed as multicomponent alloys derived based on the novel alloy design philosophy of mixing a large number (usually greater than five) of elements with equiatomic or near-equiatomic concentration [1]. Despite being featured by the presence of a large number of elements, the HEAs may yet consist of solid solution phases with simple crystal structures such as FCC (e.g., equiatomic CoCrFeMnNi [2]), BCC (HfZrTiTaNb), FCC + BCC [1], or even HCP [3, 4]. The existence of solid solution phases has been attributed to the high configurational entropy due to the mixing of a large number of elements, which can stabilize phases with simple crystal structures by decreasing the free energy sufficiently [1]. More recently, the scope of HEAs has been considerably expanded to include non-equiatomic multiphase HEAs, thereby unfolding the massive unexplored composition space existing in the hyper-dimensional phase diagrams for developing novel complex concentrated and compositionally complex alloys (CCAs) [5,6]. Meanwhile, HEAs have attracted unprecedented attention for possible usage in advanced structural applications due to their many unique and intriguing properties [7–24].

The mechanical properties of engineering alloys can be vastly enhanced by microstructural tailoring through appropriate thermo-mechanical processing (TMP) routes [25–28]. TMP routes involving deformation and thermal treatments can significantly affect the microstructure and texture of the processed materials, thereby opening the pathway for tuning the mechanical properties. Therefore, TMP aspects

* Corresponding author.
E-mail address: pinakib@msme.iith.ac.in (P.P. Bhattacharjee).

https://doi.org/10.1016/j.intermet.2020.107029
Received 22 September 2020; Received in revised form 8 November 2020; Accepted 8 November 2020
Available online 23 November 2020

of HEAs have gained considerable momentum in the last few years. Consequently, the microstructure and properties of different HEA classes are intensely investigated by a wide variety of different processing routes. In particular, the CoCrFeMnNi has been used as a model alloy due to the stable FCC structure of this HEA. The effect of various processing parameters, namely strain [29], starting grain size [30], cryo-rolling [28,31], and heating rate [32] on microstructure and texture formation during cold-rolling in the FCC equiatomic CoCrFeMnNi HEA have been clarified.

Warm-rolling of materials carried out above the cold-rolling regime but below the recrystallization temperature or hot-rolling is an attractive processing strategy for tuning microstructure and mechanical properties. In comparison to cold-rolling, the forming load is reduced, which leads to energy savings. As compared to hot-rolling, the surface finishing is considerably better in warm-rolled materials due to the reduced oxidation and scale formation [33]. In addition, warm-rolling can be effectively used for controlling microstructure and texture in aluminum, steels, and other alloys [34]. However, the effect of this processing route on microstructure, texture, and mechanical properties has been investigated only to a limited extent in HEAs. Nevertheless, the limited research investigations carried out on eutectic [35,36] and other dual-phase [37] HEAs shows the considerable potential of warm-rolling for tailoring microstructure for enhancing mechanical properties.

In the present research, we investigate the effect of warm-rolling on microstructure, texture, and mechanical properties of FCC single-phase CoCrFeMnNi HEA. To highlight the impact of warm-rolling, the results are compared with the same HEA processed previously by cold-rolling [29]. It is envisaged that the present research will be useful in understanding the effect of warm-rolling in other single-phase FCC HEAs.

2. Experimental

2.1. Processing

The experimental alloy in the form of buttons (approximately ~ 100 g) was prepared by arc melting under a protective argon atmosphere, starting with high purity elements (>99% purity). The melt was flipped and remelted for four to five times for achieving consistency in the composition. The process was followed by drop-casting in a water-cooled copper mould. The as-cast ingots with the dimensions of 75 mm (length) × 10 mm (width) × 6 mm (thickness) were further homogenized at 1100 °C for 6 h to improve the chemical homogeneity. Samples with the dimensions of 20 mm (length) × 10 mm (width) × 6 mm (thickness) were extracted from the homogenized alloy and cold-rolled to ~50% reduction in thickness (corresponding to ~3 mm thickness) using a laboratory rolling machine having roll diameter of ~140 mm (SPX precision instrument, Fenn Division, USA) and further annealed at 800 °C for 1 h in a salt bath furnace to break the coarse as-cast structure. These cold-rolled and annealed specimens (of thickness ~3 mm) were used as the starting material for further thermo-mechanical processing by warm-rolling.

The warm-rolling process was carried out at 600 °C, which was just below the recrystallization temperature of the HEA (~650 °C), as reported in the previous investigations by Bhattacharjee et al. For this purpose, the small specimens obtained from the starting cold-rolled and annealed plates (50% cold-rolled and annealed at 800 °C/1 h) were multi-pass (~16–18 passes were used) warm-rolled up to 90% reduction in thickness (corresponding to a final thickness ~300 μm). The specimens were kept in a furnace at 600 °C for 20 min before each pass. To minimize the heat loss, the rolls were preheated to ~200 °C. Rectangular strips were obtained from the 90% warm-rolled sheets and were further annealed for 1 h at temperatures varying from 600 °C to 1200 °C in a salt bath furnace.

2.2. Characterization

The phase identifications in selected bulk specimens was carried out by x-ray diffraction (XRD; Make: Rigaku, Japan and Model: Ultima IV) using Co-K_α radiation ($\lambda = 1.79$ Å), scan rate of 2° per minute, and scan step size of 0.02°. The microstructure and texture of the deformed and annealed specimens were investigated by Electron Backscatter Diffraction (EBSD) and Transmission Electron Microscopy (TEM) techniques. For this purpose, an automated EBSD system (EDAX-AMETEK Inc., USA) mounted on a scanning electron microscope equipped with a field emission gun (FEG-SEM) (JEOL-JSM 7800F, Make: JEOL, Japan), and a TEM with LaB_6 emitter was used. The EBSD specimens were prepared by careful mechanical polishing using emery papers, followed by diamond abrasive pastes, and finishing with electro-polishing using an electrolyte solution comprising of 90% ethanol and 10% perchloric acid (by volume). For the deformed materials, the scans were performed with very fine step-size ~0.04 μm. The step-size was higher for the starting and annealed materials ranging from ~0.06 μm to 2.5 μm. The EBSD dataset obtained was analyzed by TSL-OIM™ software. Several EBSD scans were acquired from the starting, deformed, and annealed specimens. These scans were merged to obtain the orientation distribution functions (ODFs) and pole figures (PFs) by imposing orthotropic symmetry and using the harmonic series expansion method (Series Rank = 22). A cut-off angle of 15° was imposed to calculate the volume fraction of the different texture components.

Further microstructural analysis of selected specimens was carried out using JEOL JEM-2100 transmission electron microscope (TEM) (200 kV), and precession electron diffraction (PED) mounted on an FEI Tecnai TEM (200 kV). The PED data was analyzed by the TSL-OIM™ (EDAX Inc., USA) software. The samples were prepared by mechanical polishing followed by ion milling (PIPS-II, Gatan Inc., USA).

The mechanical properties were evaluated by hardness (Model: DuraScan 20; Make: Emco Test, Austria) and tensile tests (Maker: Instron Inc., USA, Model: Instron 5967). The hardness tests were carried out on the rolling plane using an applied load of 500 gm-f and a dwell time of 15 s. The tensile tests were carried out with the tensile axis parallel to the rolling direction (RD) and using an initial strain rate of 10^{-3} s^{-1}. The engineering strain was measured using the digital image correlation (DIC) technique (Correlated Solutions Inc., USA).

3. Results

3.1. Microstructure and texture of warm-rolled HEA

The microstructure of the starting material obtained by initial thermo-mechanical processing comprising of 50% cold-rolling and annealing (800 °C/1 h) is shown in Fig. 1. The IPF map of the starting material (Fig. 1(a)) shows a wholly recrystallized microstructure separated by high angle boundaries (HABs; misorientation (θ)>15°; highlighted by black lines). The microstructure also shows the presence of considerable fractions of annealing twin boundaries (TBs, highlighted by yellow). The average recrystallized grain size is found to be ~10 μm. The (111) PF (Fig. 1(b)), together with the ODF (Fig. 1(c)), indicates a somewhat diffuse texture in the starting material. The ODF is overlaid with selected texture components (summarized in Table 1) for further understanding of the texture. The $\phi_2 = 0°$ section shows the presence of a weak cube component ({001}<100>) along with the ND-rotated variant ({001}<110>) of the cube component. The X-ray diffraction profiles of the starting and 90% warm-rolled materials are compared in Fig. 1(d), which shows the presence of the typical FCC peaks only and does not indicate any presence of the intermetallic σ phase.

The microstructure and texture development following 90% warm-rolling are presented in Fig. 2. The IPF map (Fig. 2(a)) obtained from a region of interest (Region I) shows the development of a predominantly lamellar banded structure subdivided by HABs along with the ND. The bands appear to contain low angle boundary (LABs;

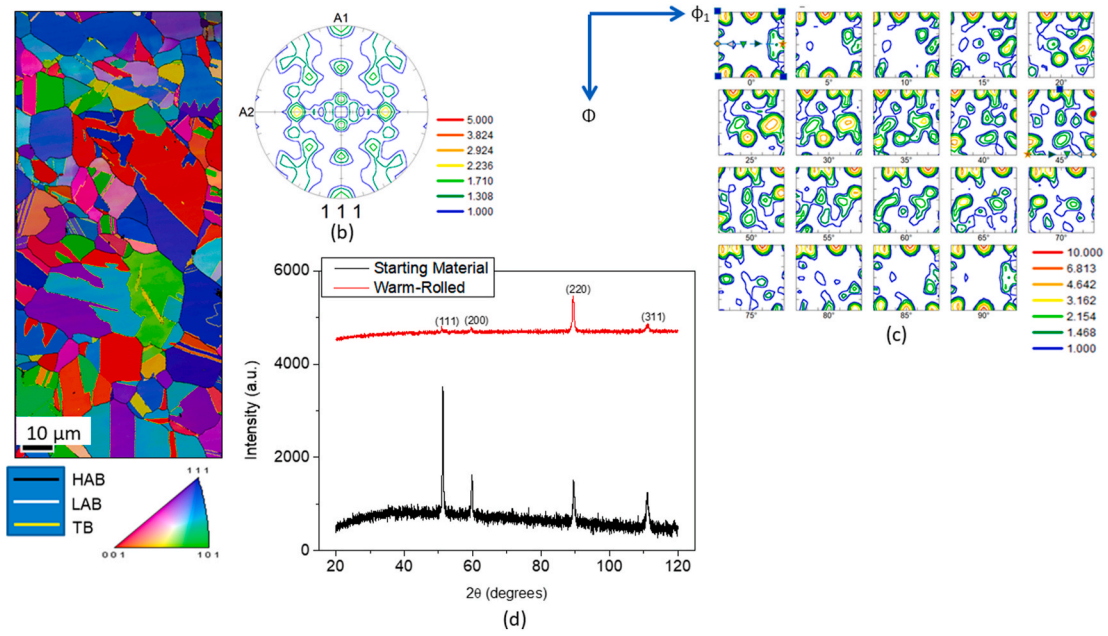

Fig. 1. (a) IPF map, (b) (111) PF, and (c) ODF of the 50% cold-rolled and annealed HEA used as the starting materials for further thermo-mechanical processing. The legends of the orientations are summarized in Table 1. (d) Compares the XRD profiles of the starting and 90% warm-rolled HEAs.

Table 1
Key deformation and recrystallization texture components in warm-rolled HEA.

Orientation	{hkl}<uvw>	(ϕ_1,Φ,ϕ_2)	Symbols
Cube (C)	{001}<100>	0, 0, 0	■
Copper (Cu)	{112}<111>	90, 35, 45	●
S	{123}<634>	59, 37, 63	▲
B	{110}<112>	35, 45, 0	▼
G	{110}<001>	0, 45, 0	◆
G/B	{110}<115>	17, 45, 0	◀
A	{110}<111>	55, 45, 0	▶

2°≤misorientation (θ)≤15°; highlighted by white lines). The average spacing between the HABs along the ND is found to be < 0.3 μm, which confirms the development of an ultrafine microstructure due to warm-rolling. The (111) PF (Fig. 2(b)) shows the development of a typical pure metal or copper type deformation texture, which is further substantiated by the relevant ODF sections ($\phi_2 = 0°$, 45°, and 65°) in Fig. 2 (c). The $\phi_2 = 0°$ section of the ODF shows strong intensity at the G/B location, while the $\phi_2 = 45°$ section shows the presence of a prominent copper component with very comparable intensity levels. Meanwhile, the $\phi_2 = 65°$ section shows the presence of a distinct S ({123}<634>) component.

The IPF map (Fig. 2(d)) obtained from another region (Region II); although it shows a lamellar structure, the bands are not as extended as the bands in Region I. Nevertheless, the bands are separated by HABs with a profuse internal LAB network. The (111) PF (Fig. 2(e)) shows a pure metal type texture with a weaker brass component. The texture development is further understood from the ODF (Fig. 2(f)). The $\phi_2 = 0°$ section of the ODF shows an intensity peak at the G/B location ({110}<115>) midway between the G ({110}<001>) and B ({110}<112>) orientations. The $\phi_2 = 45°$ and $\phi_2 = 65°$ sections confirm the presence of the strong Cu and S components, respectively.

The microstructure of the warm-rolled HEA is further investigated using TEM and PED techniques. The TEM micrograph (Fig. 3(a)) obtained from the ND-RD section shows the banded structure, which appears to contain dislocation debris inside the deformed lamellar bands. The image quality (IQ) map (Fig. 3(b)) obtained from the ND-RD section using the precession electron diffraction (PED) technique again corroborates with the lamellar structure. The IQ map also shows the presence of a tiny grain (~0.5 μm) bounded by HAGBs from all sides. The corresponding kernel average misorientation (KAM) map of the IQ map (in Fig. 3(b)) is shown in Fig. 3(c). High KAM values indicate the presence of misorientations, which in other words, signify the presence of deformation structure. The KAM map displays a very heterogeneous distribution of misorientation, featured by the presence of bands with low KAM regions (highlighted in blue) adjacent to bands having high KAM (highlighted in green). Further, the internal misorientation profile in a selected band and the tiny grain are determined along with the white and black arrows, respectively. The misorientation profiles plotted in Fig. 3(d) and (e) determined along the white and black arrows, respectively, show low point-to-point misorientation but the presence of remarkable point-to-origin or cumulative misorientation.

It may be interesting to compare the microstructure and texture of the cold-rolled HEA deformed to 90% reduction in thickness reported by Bhattacharjee et al. [29]. The TEM micrograph (Fig. 4(a)) and the associated selected area diffraction pattern (SADP) (shown inset in Fig. 4 (a)) show a nanoscale structure with HAB spacing ~30 nm. The (111) PF of the cold-rolled HEA (Fig. 4(b)) shows a predominantly brass type texture as opposed to a pure metal type texture in the warm-rolled HEA. These remarkable differences in texture could be further understood quantitatively from Fig. 4(c). The cold-rolled HEA shows a stronger B component as compared to the Cu and S components, whereas the warm-rolled HEA shows a significantly stronger S component as compared to the B component.

3.2. *Microstructure and texture after annealing*

The microstructural changes upon annealing of the 90% warm-rolled HEA are shown in Fig. 5. The IPF map (Fig. 5(a)) of the specimen treated for 700 °C/1 h shows the presence of the deformed structure, amply corroborated by the presence of a LAB network. The near-complete absence of recrystallized grains indicates that recrystallization is yet to

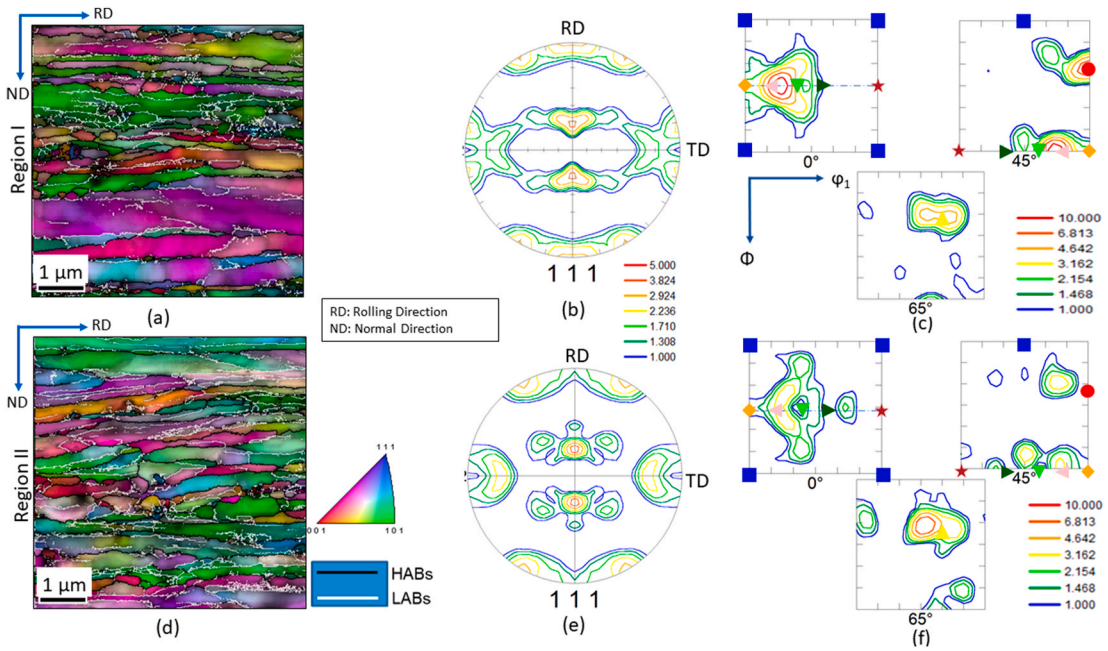

Fig. 2. ((a), (d)) IPF maps, ((b), (e)) (111) PFs and ((c), (f)) $\phi_2 = 0°$, 45° and 65° sections of the ODFs of the HEA warm-rolled to 90% reduction in thickness at 600 °C obtained from two different regions, namely Region I ((a)–(c)) and Region II ((d)–(f)). The legends of the orientations are summarized in Table 1.

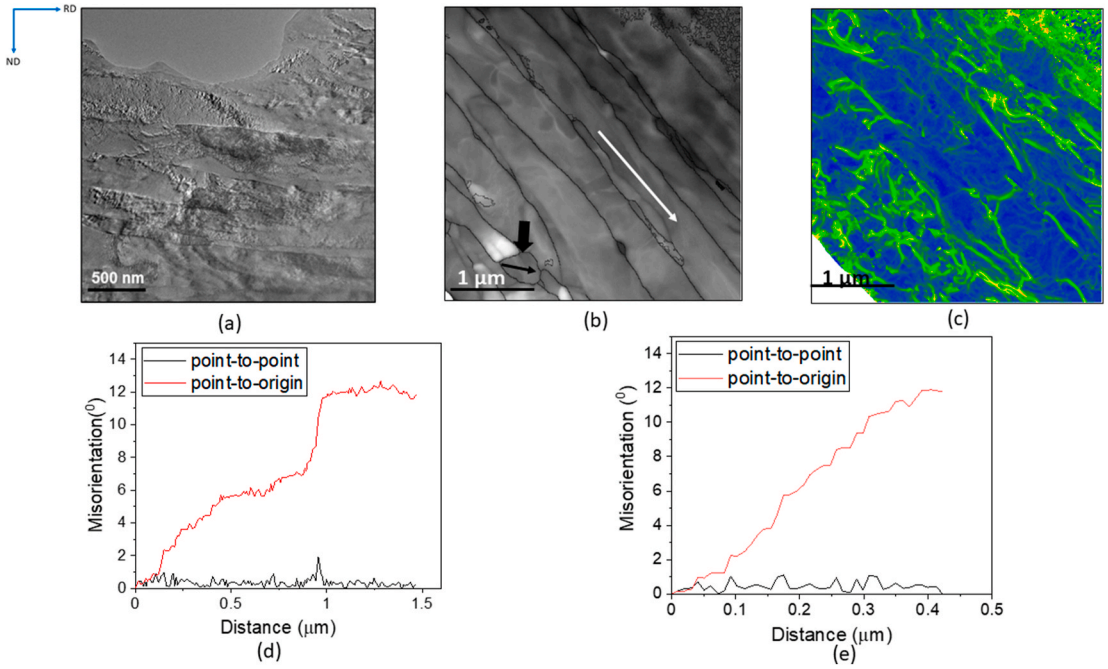

Fig. 3. (a) TEM micrograph, (b) PED-IQ map, and (c) KAM map of the 90% warm-rolled HEA. (d) and (e) show the misorientation profiles along the white and black arrows in (b), respectively.

start in the warm-rolled material; however, the (111) PF (Fig. 5(d)) suggests that the deformation texture is sharpened. The IPF map (Fig. 5 (b)) following annealing treatment for 750 °C/1 h results in complete recrystallization so that the microstructure consists of equiaxed recrystallized grains completely bounded by HABs with profuse annealing twins. The associated (111) PF appears weakened with scattered intensities (Fig. 5(e)). The IPF map of the specimen treated for 800 °C/1 h (Fig. 5(c)) does not show any significant changes compared to that of the specimen treated for 750 °C/1 h. The (111) PF (Fig. 5(f)) also appears very similar to that of the specimen treated for 750 °C/1 h.

The evolution of microstructure and texture following annealing at higher temperatures is represented in Fig. 6. Increasing annealing temperature results in a consistent increase in grain size, which can be quickly confirmed from the IPF maps of the HEA annealed at 900 °C (Fig. 6(a)), 1000 °C (Fig. 6(b)), and 1200 °C (Fig. 6(c)). Profuse annealing twins could be identified in all the IPF maps. The (111) PFs of the three annealed materials (Fig. 6(d), (e), and Fig.6(f)) indicate the retention of deformation texture components.

The changes in texture with increasing annealing temperature can be further understood from the ODFs of the different annealed materials in

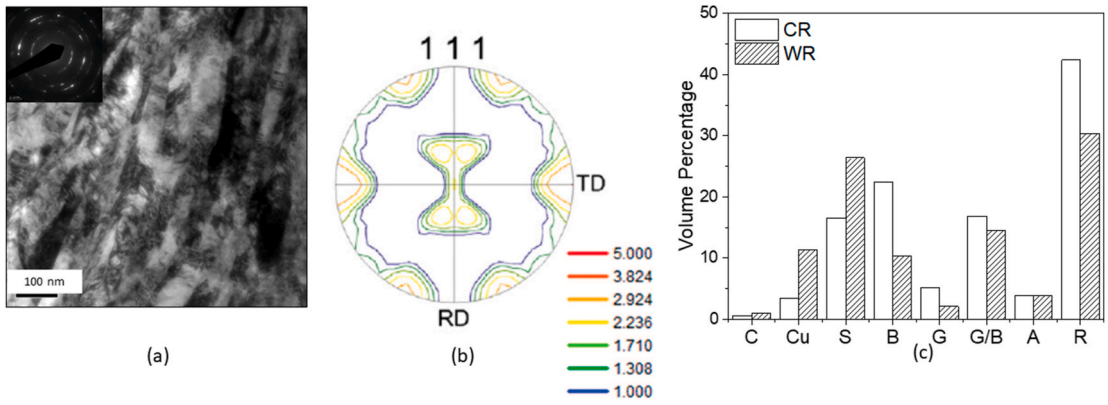

Fig. 4. (a) TEM micrograph (inset shows selected area diffraction pattern), (b) (111) PF of the 90% cold-rolled HEA. (c) Shows the quantitative comparison of the typical texture components in the 90% cold- and warm-rolled HEA (WR and CR stand for warm- and cold-rolled materials). The data for cold-rolled HEA is obtained from reference [29,38].

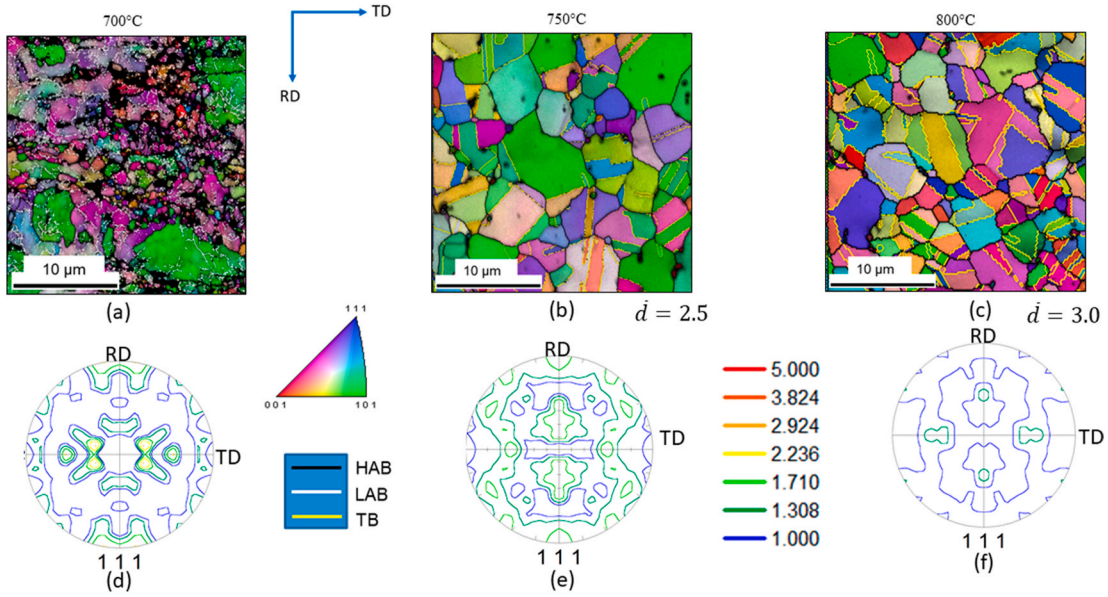

Fig. 5. (a) through (c) are the IPF maps of the 90% warm-rolled HEA annealed at (a) 700 °C, (b) 750 °C, and (c) 800 °C for 1 h. (d) Through (f) show the corresponding (111) PFs.

Fig. 7. The $\phi_2 = 0°$, 35°, 45°, and 65° sections of the ODFs of the specimens annealed at 750 °C (Fig. 7(a)) and 800 °C (Fig. 7(b)) show the presence of orientations along the α-fiber (ND//<110>, running from the G to the rotated-G orientation through the B orientation). However, perceptible scatter of orientations could be easily recognized. The $\phi_2 = 0°$ section of the ODF of the 900 °C (Fig. 7(c)) and 1000 °C (Fig. 7(d)) annealed material shows intensity cantered around the G component, while the $\phi_2 = 0°$ section of the ODF of the 1200 °C (Fig. 7(e)) indicates the presence of orientations along the α-fiber. The $\phi_2 = 35°$ sections of the different annealed specimens do not reveal the presence of a prominent BR component. The $\phi_2 = 45°$ sections of the ODFs shows weak Cu component except the specimen annealed at 900 °C. The $\phi_2 = 65°$ sections of the ODFs shows a considerable weakening of the S component (which was relatively strong in the warm-rolled specimen) after annealing. Overall, the texture is weakened after annealing at different temperatures.

The microstructural development during annealing is further analyzed quantitatively in Fig. 8. The variation in recrystallized grain size with annealing temperature is represented in Fig. 8(a) and compared with the grain size in the cold-rolled and annealed HEA reported previously by Bhattacharjee et al. [29] up to an annealing temperature of 1000 °C. It is noted that the average grain size in the warm-rolled and annealed HEA was consistently much higher than that of the cold-rolled and annealed HEA. The average grain size values in the cold-rolled and warm-rolled HEA following annealing at 900 °C are ~3 μm and ~20 μm, respectively. After annealing at 1000 °C, the average grain size values of the warm-rolled HEA are ~40 μm, which is twice than that of the cold-rolled HEA ~20 μm.

The misorientation angle distribution of the different annealed materials (Fig. 8(b)) shows a strong peak at 60°, which corresponds to the profuse Σ3 annealing TBs present in the microstructure. For further understanding, the variation of the Grain Boundary Character Distribution (GBCD) elucidating the fractions of the LABs, HABs, and TBs in the different warm-rolled and annealed HEAs are shown in Fig. 8(c). At lower annealing temperatures, the TB fractions do not differ significantly. However, at higher annealing temperatures where significant grain growth occurs, the TB fraction increases perceptibly. This could be clearly understood from the higher TB fractions obtained in the HEA specimens annealed at 1000 °C and 1200 °C. A very similar trend in the GBCD variation has been reported for the cold-rolled and annealed HEA [29].

The texture development in the warm-rolled and annealed HEA is

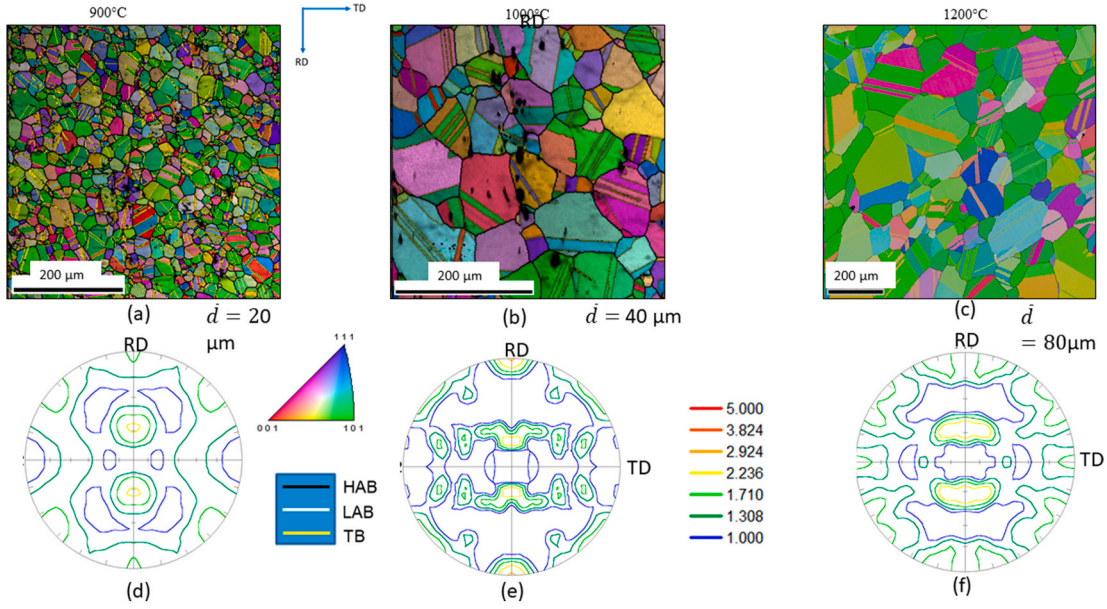

Fig. 6. ((a)–(c)) IPF maps and ((d)–(f)) (111) PFs of the 90% warm-rolled HEA annealed at ((a), (d)) 900 °C, ((b), (e)) 1000 °C and ((c), (f)) 1200 °C for 1 h.

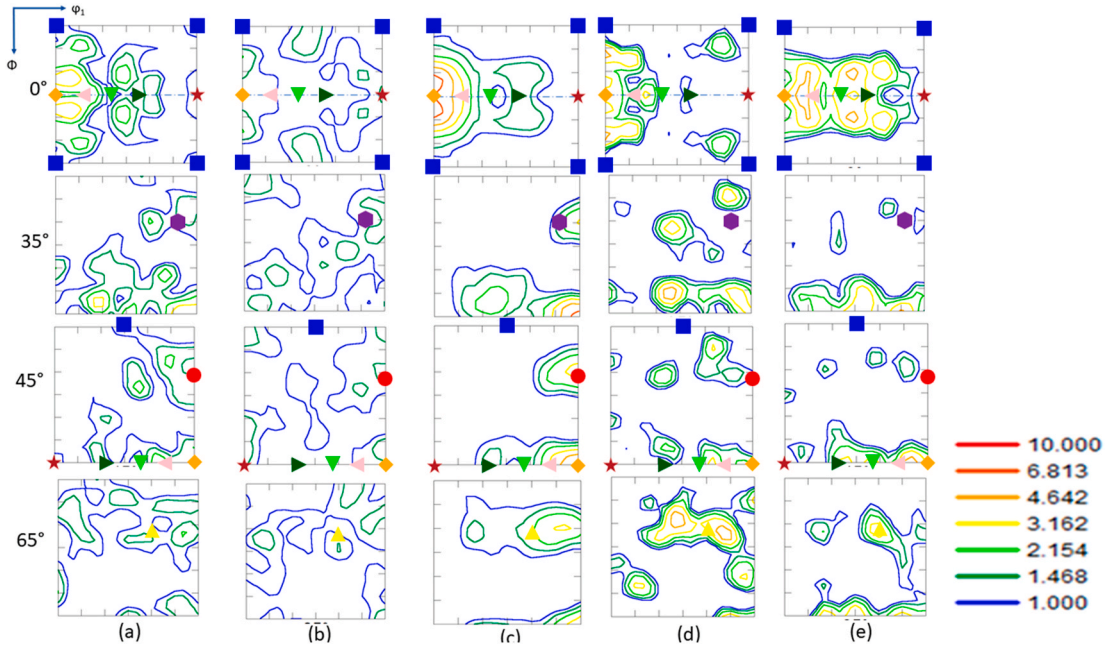

Fig. 7. $\phi_2 = 0°$, 35°, 45° and 65° sections of the ODFs of the 90% warm-rolled HEA annealed at (a) 750 °C, (b) 800 °C, (c) 900 °C, (d) 1000 °C and (e) 1200 °C for 1 h. The legends of the symbols used for the different orientations are summarized in Table 1.

compared with their cold-rolled and annealed counterparts reported by Bhattacharjee et al. [29] For this purpose, the volume fractions of the Cu, S, and total volume fraction of the α-fiber components (sum of the volume fractions of the orientations along the α-fiber summarized in Table 1) in the cold- and warm-rolled condition and after treating at 800 °C, 900 °C, and 1000 °C for 1 h are considered for comparison (Fig. 9). The volume fraction of the α-fiber in the cold-rolled specimen is significantly decreased after annealing, indicating a weakening of the texture. On the other hand, the volume fraction of the strong S component in the deformation texture of the warm-rolled HEA is considerably diminished after annealing. Meanwhile, the volume fraction of the α-fiber is also decreased after annealing (albeit the slight increase in the 900 °C annealed condition). Therefore, the texture is weakened after annealing in the warm-rolled HEA, like the behavior observed for the cold-rolled HEA.

The mechanical properties of the warm-rolled and annealed specimens are evaluated using hardness (Fig. 10(a)) and tensile tests (Fig. 10 (b)). The hardness of the warm-rolled HEA is ~380 Hv, which decreases consistently with increasing annealing temperature. The hardness of the specimen treated at 750 °C (where a completely recrystallized fine-grained microstructure is obtained) is ~213 Hv. Annealing at temperatures of 900 °C and beyond results in low hardness values. Consequently, tensile properties were only compared for the as-cast, warm-rolled, and after annealing at 600 °C (which corresponds to deformed state) and 750 °C (corresponding to completely recrystallized state). The starting material shows low strength but high elongation. Warm-rolling results in a considerable enhancement in strength but at the expense of ductility. Annealing at 600 °C results in a decrease in strength, with only

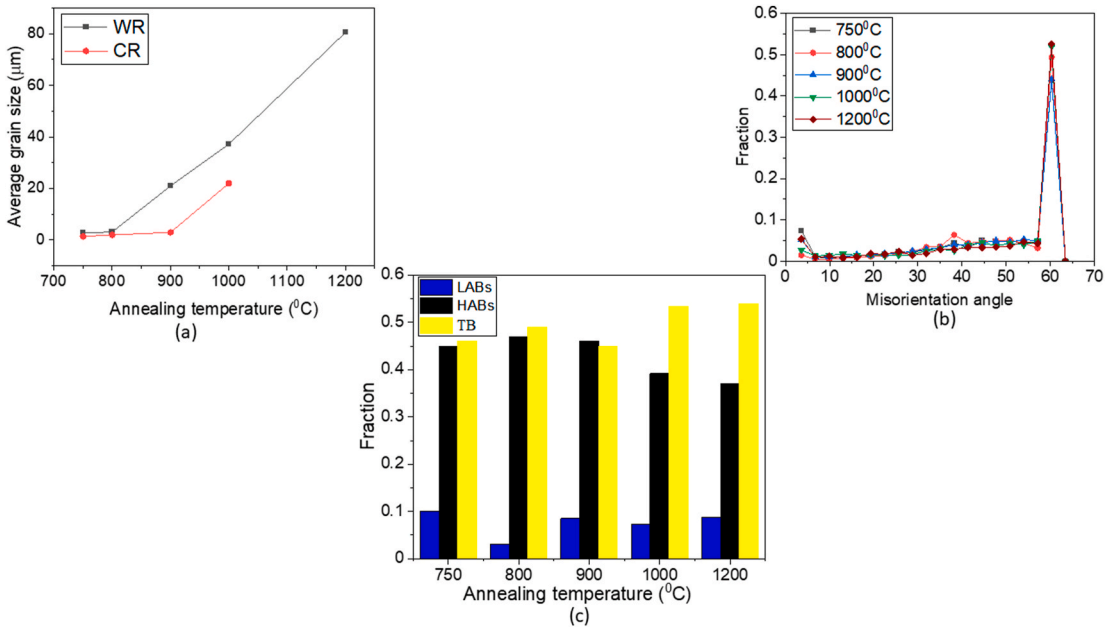

Fig. 8. Variation of (a) average grain size (CR and WR indicate cold- and warm-rolling, respectively. The data for cold-rolled and annealed HEA is obtained from Ref. [29]) (b) misorientation angle distribution and (c) grain boundary character distribution in the warm-rolled HEA with annealing temperature (the data for cold-rolled HEA is obtained from Refs. [29]).

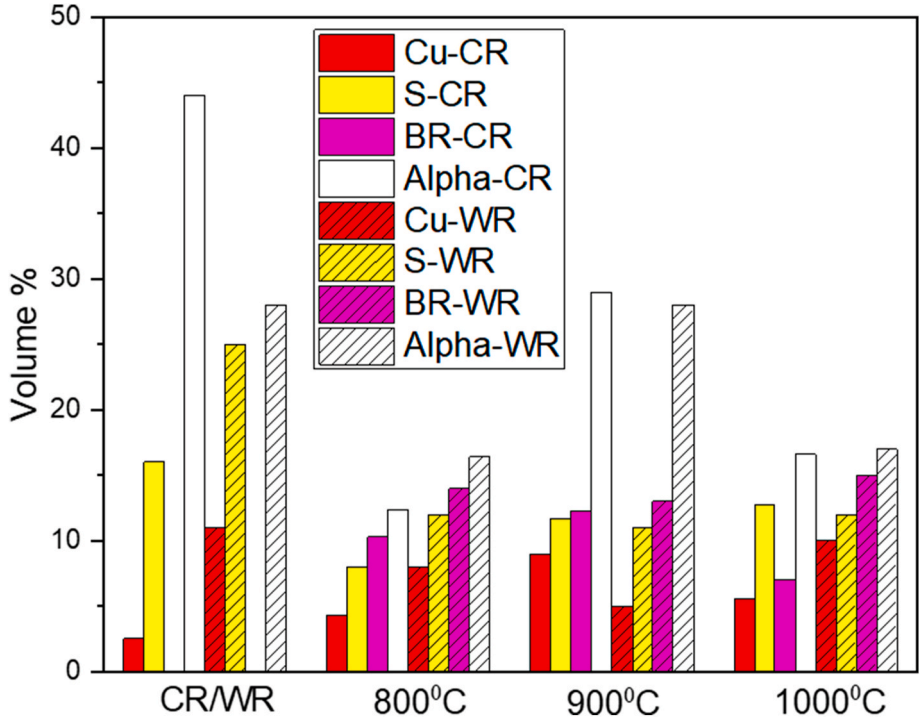

Fig. 9. Comparison of the key texture components in the cold- and warm-rolled HEA deformed and annealed at different temperatures (CR and WR indicate cold- and warm-rolling, respectively. E.g. Cu-CR and Cu-WR indicate Cu component in the cold- and warm-rolled HEAs, respectively).

marginal improvement in ductility. Meanwhile, annealing at 750 °C results in an improved strength ductility combination featured by YS~710 MPa, UTS~815 MPa, and elongation to failure~16%.

4. Discussion

The significant observations concerning the effect of severe warm-rolling are the formation of a predominantly lamellar structure and copper type deformation texture. The formation of a deformation-induced ultrafine lamellar deformation structure has been widely reported in different FCC metals and alloys and attributed to the grain subdivision mechanism [39,40]. It has been argued that the equiaxed grains in the starting material are subdivided by the lamellar HABs on an increasingly finer scale with increasing deformation. The processes governing the generation of ultrafine and nanoscale lamellar structure could be accompanied by microstructural and textural changes. The

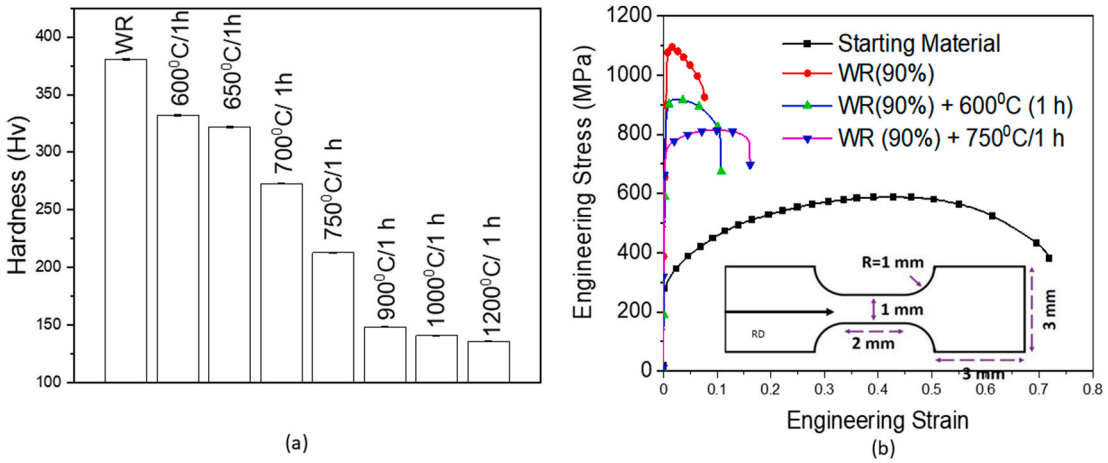

Fig. 10. (a) shows the hardness variation of deformed and annealed specimens. (b) Shows the tensile properties of the selected specimens (WR (90%) indicates the 90% warm-rolled specimen).

microstructural processes might involve the formation of the LAB dominated cell and sub-grain structure at early stages of deformation, a gradual increase in the misorientation angle of the cell/sub-boundaries with increasing deformation by the accumulation of the dislocation at the boundaries, and final conversion of the LABs into random HABs. On the other hand, from the point of view of texture evolution, the grain subdivision process could lead to the rotation of different parts of grains to different stable end orientations owing to the selection of different slip systems, thereby leading to the macroscopic division of grains by deformation bands and microscopic subdivision in increasingly finer scale by the HABs [39,40].

Nevertheless, the warm-rolled HEA differs considerably from its cold-rolled counterpart with respect to microstructure and texture evolution. The warm-rolled HEA shows a much larger HAB spacing ~300 nm than the nanoscale structure in the cold-rolled HEA with HAB spacing ~30 nm. These remarkable differences in microstructure could be accounted for by the dynamic annihilation of dislocations during severe warm-rolling by the process of climb or cross-slip. The annihilation of dislocations is amply corroborated by the high fraction of the low KAM regions in the as warm-rolled deformation structure and low point to point misorientation (typical for a sub-grain structure), but rather large cumulative misorientation indicating progressively misoriented sub-grains. The annihilation of dislocations could effectively diminish the dislocation population available for accumulation at the LABs for converting them into random HABs. Therefore, the creation of the deformation-induced HABs is significantly inhibited in the warm-rolled HEA, thus leading to a much larger HAB spacing than that in the cold-rolled HEA.

Meanwhile, the deformation texture of the warm-rolled HEA is featured by a pure metal type or copper type texture as opposed to a predominantly brass type texture in the cold-rolled HEA. The texture transition from pure metal type to brass type texture with decreasing SFE has been extensively investigated in different alloy systems [41]. Therefore, the evolution of a brass type deformation texture is characteristic of the low SFE materials [42] and is consistent with the recent theoretical [43] and experimental [44] reports. Although the mechanism of texture transition is yet to be fully clarified, mechanisms involving extensive twin and shear bands formation have been intensely debated [41,45]. It is noteworthy that the SFE of the CoCrFeMnNi HEA shows a strong temperature dependence, increasing with increasing temperature [46]. At the warm-rolling temperature, the increased SFE of the HEA favors deformation by dislocation slip over deformation by twinning. At the same time, unlike deformation by cold-rolling, the rather homogeneous deformation at the elevated temperature of warm-rolling could effectively suppress the propensity for the formation of extensive shear bands. These factors amply justify the development of predominantly pure metal or copper type texture in the warm-rolled HEA.

The previous studies by Bhattacharjee et al. [29] on the 90% cold-rolled HEA revealed that recrystallization already occurs at 650 °C, whereas a completely recrystallized microstructure can be obtained only after treating for 700 °C/1 h. Considering the liquidus temperature of the HEA ~1339 °C (1612 K), the annealing temperature of 700 °C (973 K) results in a homologous temperature of $\sim 0.61 \times T_m$, which is decidedly higher than the upper bound of recrystallization temperature $\sim 0.50 \times T_m$ [29]. In the warm-rolled material, a completely recrystallized microstructure is obtained even at a higher annealing temperature ~750 °C (1023 K).

It is noteworthy that the cold-rolling results in a much finer microstructure (the HAB spacing <50 nm is almost an order of magnitude lower than that in the warm-rolled HEA ~300 nm). Besides, the cold-rolled microstructure is also featured by a high density of deformation heterogeneities such as shear bands [29]. On the other hand, warm-rolling leads to dynamic annihilation of dislocations, leading to a diminished driving force for static recrystallization. Therefore, the cold-rolled microstructure has a perceptibly higher driving force for recrystallization and greater density of the potential nucleation sites. These characteristic differences lead to higher recrystallization temperature in the warm-rolled HEA. At the same time, due to a lower density of nucleation sites, grain growth dominates in the warm-rolled material, which leads to a consistently larger recrystallized grain size in the warm-rolled HEA. While this difference in grain size is quite evident even at lower annealing temperature, at higher annealing temperatures where substantial grain growth may occur readily, the difference in grain size with similarly treated cold-rolled HEA is remarkable.

Annealing of the warm-rolled HEA also results in a perceptible change in grain boundary character distribution distinguished by the generation of a high fraction of TBs, similar to the behavior observed in a wide range of medium to low SFE alloys [47,48]. The fraction of TBs appears to further increase with increasing annealing temperature during grain growth, mainly at the expense of the random HABs. The fraction of the LABs is not significantly affected. Such a pattern in the evolution of the boundary pattern is also shown by the cold-rolled HEA. It is noted that the driving force for grain growth is the total reduction in the grain boundary energy. Since the boundary energy of the Σ3 TB is significantly lower than the random HABs [49], the formation of TBs at the expense of random HABs are favored to minimize the overall boundary energy.

The recrystallization textures of the cold- [29] or even cryo-rolled

[31] HEA investigated by Bhattacharjee et al. reveal the retention of the deformation texture components. While a brass dominated texture has been universally reported by different cold-rolled low SFE materials [41], the recrystallization texture shows considerable differences. Heavily cold-rolled low SFE brass shows a strong BR component ({236}<385>) upon annealing, which is strongly affected by various annealing parameters. The origin of a strong brass component has been attributed to mechanisms involving preferential nucleation, subsequent twinning, and growth owing to a high mobility 40°<111> relationship with the B, which is the main component of the deformation texture. In contrast, the cold-rolled low SFE CoCrFeMnNi shows the retention of deformation texture, namely the α-fiber components (including G, G/B, and B) [29] so that the recrystallization texture is a random sampling of the deformation texture components, similar to the behavior observed in certain authentic and TWIP steels [50–52]. Thus, the formation of recrystallization texture in the cold-rolled HEA is essentially featured by the absence of preferential nucleation and growth.

In the present case, the deformation texture of the warm-rolled HEA is a predominantly pure metal or copper type texture, similar to heavily cold-rolled medium to high SFE materials. However, unlike the typically strong and sharp cube texture observed in heavily cold-rolled and annealed medium to high SFE materials, the recrystallization texture of the warm-rolled HEA shows considerable weakening. The origin of cube texture has been considered from the point of view of preferential nucleation (due to the pre-recovered structure of the cube bands) or preferential growth (due to the high mobility misorientation relationship with the surrounding S orientation). Nevertheless, the weakening of the recrystallization texture precludes the role of strong preferential nucleation or growth; a pattern also observed for cold-rolled HEA even though the starting deformation textures are significantly different. In essence, irrespective of the different deformation texture in the cold-[29] and warm-rolled HEAs, the recrystallization texture formation is featured by the absence of strong preferential nucleation or growth.

The hardness variation in the warm-rolled and annealed HEA shows the usual behavior, decreasing with increasing annealing temperature. In good agreement, the warm-rolled and materials annealed below the recrystallization temperature shows high strength but very limited tensile elongation. The material treated for 750 °C/1 h, which yields a fine-grained, fully recrystallized microstructure, shows an impressive strength-ductility balance. Further, the weakening of recrystallization texture is expected to diminish anisotropy in mechanical properties. Evidently, thermo-mechanical processing by warm-rolling can considerably improve the mechanical properties of CoCrFeMnNi HEA.

5. Conclusions

In the present research, FCC equiatomic CoCrFeMnNi HEA was thermo-mechanically processed by severe warm-rolling and annealing. The following conclusions may be drawn from the present study:

(i) Warm-rolling to 90% reduction in thickness resulted in a predominantly lamellar microstructure, which was an order of magnitude coarser than the similarly cold-rolled HEA. The significantly coarser microstructure in the warm-rolled HEA could be attributed to the dynamic annihilation of dislocations during deformation.

(ii) Warm-rolling results in the development of pure metal or copper type texture as opposed to a predominantly brass type texture in the cold-rolled HEA. The stark differences in the deformation texture could be attributed to the increase in the SFE, which promotes more homogeneous deformation by dislocation slip over deformation by nano-twinning or extensive shear band formation.

(iii) The lower stored energy due to dynamic annihilation of dislocations and coarser deformation structure of the warm-rolled material resulted in higher recrystallization temperature, and coarser recrystallized grain size.

(iv) Annealing resulted in the weakening of the recrystallization texture. The recrystallization texture formation indicated the absence of strong preferential nucleation or growth.

(v) The HEA warm-rolled and annealed at 750 °C, which yielded a fine-grained, completely recrystallized microstructure with an optimum strength-ductility combination. In summary, the present results demonstrated that warm-rolling could be effectively used as a processing tool for tailoring microstructure and properties of CoCrFeMnNi HEA.

CRediT authorship contribution statement

J. Saha: Investigation, Formal analysis, Writing - original draft. **G. Ummethala:** Investigation. **S.R.K. Malladi:** Investigation, Supervision, Project administration, Supervision, Writing - review & editing, Funding acquisition. **P.P. Bhattacharjee:** Conceptualization, Methodology, Formal analysis, Writing - review & editing, Supervision, Project administration, Funding acquisition.

Declaration of competing interest

The authors declare that they have no known competing financial interests or personal relationships that could have appeared to influence the work reported in this paper.

Acknowledgments

The authors would like to acknowledge the financial support of DST-SERB, India (under grant no. EMR/2016/002215 and ECR/2017/002628), DST-FIST program (under grant no. SR/FST/ETI-421/2016), and the DRDO (ER&IPR) (under grant no. ERIP/ER/2002002/M/01/1773). The support of Dr. Vajinder Singh (DMRL, Hyderabad) for the PED measurements and the kind permission of Dr. Partha Ghosal (DMRL, Hyderabad) to carry out the measurements are gratefully acknowledged. P.P. Bhattacharjee would also like to sincerely acknowledge Professor J.W. Yeh, Dr. C.W. Tsai, and Chi Lee (NTHU, Taiwan) for the previous collaboration pertaining to cold-rolling studies on the alloy.

References

[1] J.W. Yeh, S.K. Chen, S.J. Lin, J.Y. Gan, T.S. Chin, T.T. Shun, C.H. Tsau, S.Y. Chang, Nanostructured high-entropy alloys with multiple principal elements: novel alloy design concepts and outcomes, Adv. Eng. Mater. 6 (2004) 299–303.
[2] B. Cantor, I.T.H. Chang, P. Knight, A.J.B. Vincent, Microstructural development in equiatomic multicomponent alloys, Mater. Sci. Eng., A 375–377 (2004) 213–218.
[3] Y.J. Zhao, J.W. Qiao, S.G. Ma, M.C. Gao, H.J. Yang, M.W. Chen, Y. Zhang, A hexagonal close-packed high-entropy alloy: the effect of entropy, Mater. Des. 96 (2016) 10–15.
[4] A. Takeuchi, K. Amiya, T. Wada, K. Yubuta, W. Zhang, High-entropy alloys with a hexagonal close-packed structure designed by equi-atomic alloy strategy and binary phase diagrams, JOM (J. Occup. Med.) 66 (2014) 1984–1992.
[5] S. Gorsse, D.B. Miracle, O.N. Senkov, Mapping the world of complex concentrated alloys, Acta Mater. 135 (2017) 177–187.
[6] D.B. Miracle, O.N. Senkov, A critical review of high entropy alloys and related concepts, Acta Mater. 122 (2017) 448–511.
[7] Y. Zhang, T.T. Zuo, Z. Tang, M.C. Gao, K.A. Dahmen, P.K. Liaw, Z.P. Lu, Microstructures and properties of high-entropy alloys, Prog. Mater. Sci. 61 (2014) 1–93.
[8] B. Gludovatz, A. Hohenwarter, D. Catoor, E.H. Chang, E.P. George, R.O. Ritchie, A fracture-resistant high-entropy alloy for cryogenic applications, Science 6201 (2014) 1153–1158.
[9] M.H. Tsai, J.W. Yeh, High-entropy alloys: a critical review, Mater. Res. Lett. 2 (2014) 107–123.
[10] E.P. George, D. Raabe, R.O. Ritchie, High-entropy alloys, Nat. Rev. Mater. 4 (2019) 515–534.
[11] E.P. George, W.A. Curtin, C.C. Tasan, High entropy alloys: a focused review of mechanical properties and deformation mechanisms, Acta Mater. 188 (2020) 435–474.
[12] D.B. Miracle, High entropy alloys as a bold step forward in alloy development, Nat. Commun. 10 (2019) 1805.

[13] E.J. Pickering, N.G. Jones, High-entropy alloys: a critical assessment of their founding principles and future prospects, Int. Mater. Rev. 61 (2016) 183–202.
[14] B.S. Murty, J.W. Yeh, S. Ranganathan, P.P. Bhattacharjee, High-entropy Alloys, second ed.s., Elsevier, 2019.
[15] Z. Lei, X. Liu, Y. Wu, H. Wang, S. Jiang, S. Wang, X. Hui, Y. Wu, B. Gault, P. Kontis, D. Raabe, L. Gu, Q. Zhang, H. Chen, H. Wang, J. Liu, K. An, Q. Zeng, T.G. Nieh, Z. Lu, Enhanced strength and ductility in a high-entropy alloy via ordered oxygen complexes, Nature 563 (2018) 546–550.
[16] H.Y. Diao, R. Feng, K.A. Dahmen, P.K. Liaw, Fundamental deformation behavior in high-entropy alloys: an overview, Curr. Opin. Solid State Mater. Sci. 21 (2017) 252–266.
[17] W. Lu, C.H. Liebscher, G. Dehm, D. Raabe, Z. Li, Bidirectional transformation enables hierarchical nanolaminate dual-phase high-entropy alloys, Adv. Mater. 30 (2018) 1804727.
[18] P. Sathiyamoorthi, H.S. Kim, High-entropy alloys with heterogeneous microstructure: processing and mechanical properties, Prog. Mater. Sci. (2020) 100709.
[19] J.W. Yeh, S.J. Lin, Breakthrough applications of high-entropy materials, J. Mater. Res. (2018) 1–9.
[20] Z. Li, K.G. Pradeep, Y. Deng, D. Raabe, C.C. Tasan, Metastable high-entropy dual-phase alloys overcome the strength-ductility trade-off, Nature 534 (2016) 227–230.
[21] M. Komarasamy, T. Wang, K. Liu, L.R. Nieto, R.S. Mishra, Hierarchical multi-phase microstructural architecture for exceptional strength-ductility combination in a complex concentrated alloy via high-temperature severe plastic deformation, Scripta Mater. 162 (2019) 38–43.
[22] Z. Lei, Y. Wu, J. He, X. Liu, H. Wang, S. Jiang, L. Gu, Q. Zhang, B. Gault, D. Raabe, Z. Lu, Snoek-type damping performance in strong and ductile high-entropy alloys, Sci. Adv. 6 (2020), eaba7802.
[23] Z. Fu, L. Jian, J.L. Wardini, B.E. MacDonald, H. Wen, W. Xiong, D. Zhang, Y. Zhou, T.J. Rupert, W. Chen, E.J. Lavernia, A high-entropy alloy with hierarchical nanoprecipitates and ultrahigh strength, Sci. Adv. 4 (2018), eaat8712.
[24] A.S. Tirunilai, J. Sas, K.P. Weiss, H. Chen, D.V. Szabó, S. Schlabach, S. Haas, D. Geissler, J. Freudenberger, M. Heilmaier, A. Kauffmann, Peculiarities of deformation of CoCrFeMnNi at cryogenic temperatures, J. Mater. Res. (2018) 1–14.
[25] F. Otto, N.L. Hanold, E.P. George, Microstructural evolution after thermomechanical processing in an equiatomic, single-phase CoCrFeMnNi high-entropy alloy with special focus on twin boundaries, Intermetallics 54 (2014) 39–48.
[26] D.G. Shaysultanov, N.D. Stepanov, A.V. Kuznetsov, G.A. Salishchev, O.N. Senkov, Phase composition and superplastic behavior of a wrought AlCoCrCuFeNi highentropy alloy, JOM (J. Occup. Med.) 65 (2013) 1815–1828.
[27] A.V. Kuznetsov, D.G. Shaysultanov, N.D. Stepanov, G.A. Salishchev, O.N. Senkov, Tensile properties of an AlCrCuNiFeCo high-entropy alloy in as-cast and wrought conditions, Mater. Sci. Eng., A 533 (2012) 107–118.
[28] N. Stepanov, M. Tikhonovsky, N. Yurchenko, D. Zyabkin, M. Klimova, S. Zherebtsov, A. Efimov, G. Salishchev, Effect of cryo-deformation on structure and properties of CoCrFeNiMn high-entropy alloy, Intermetallics 59 (2015) 8–17.
[29] P.P. Bhattacharjee, G.D. Sathiaraj, M. Zaid, J.R. Gatti, C. Lee, C.W. Tsai, J.W. Yeh, Microstructure and texture evolution during annealing of equiatomic CoCrFeMnNi high-entropy alloy, J. Alloys Compd. 587 (2014) 544–552.
[30] G.D. Sathiaraj, P.P. Bhattacharjee, Effect of starting grain size on the evolution of microstructure and texture during thermo-mechanical processing of CoCrFeMnNi high entropy alloy, J. Alloys Compd. 647 (2015) 82–96.
[31] G.D. Sathiaraj, P.P. Bhattacharjee, C.W. Tsai, J.W. Yeh, Effect of heavy cryo-rolling on the evolution of microstructure and texture during annealing of equiatomic CoCrFeMnNi high entropy alloy, Intermetallics 69 (2016) 1–9.
[32] G.D. Sathiaraj, C.W. Tsai, J.W. Yeh, M. Jahazi, P.P. Bhattacharjee, The effect of heating rate on microstructure and texture formation during annealing of heavily cold-rolled equiatomic CoCrFeMnNi high entropy alloy, J. Alloys Compd. 688 (2016) 752–761.
[33] G.E. Dieter, Mechanical Metallurgy, McGraw-Hill, 1989.
[34] B. Verlinden, J. Driver, I. Samajdar, R.D. Doherty, Thermo-mechanical Processing of Metallic Materials, Elsevier Science, Oxford, 2007.
[35] S.R. Reddy, S. Yoshida, U. Sunkari, A. Lozinko, J. Joseph, R. Saha, D. Fabijanic, S. Guo, P.P. Bhattacharjeea, N. Tsuji, Engineering heterogeneous microstructure by severe warm-rolling for enhancing strength-ductility synergy in eutectic high entropy alloys, Mater. Sci. Eng., A 764 (2019) 138226.
[36] S.R. Reddy, S. Yoshida, T. Bhattacharjee, N. Sake, A. Lozinko, S. Guo, P. P. Bhattacharjee, N. Tsuji, Nanostructuring with structural-compositional dual heterogeneities enhances strength-ductility synergy in eutectic high entropy alloy, Sci. Rep. 9 (2019) 11505.
[37] I.S. Wani, G.D. Sathiaraj, M.Z. Ahmed, S.R. Reddy, P.P. Bhattacharjee, Evolution of microstructure and texture during thermo-mechanical processing of a two phase Al0.5CoCrFeMnNi high entropy alloy, Mater. Char. 118 (2016) 417–424.
[38] G.D. Sathiaraj, IIT Hyderabad, PhD Dissertation, 2016.
[39] B. Bay, N. Hansen, D.A. Hughes, D.K. Wilsdorf, Overview No-96 - evolution of fcc deformation structures in polyslip, Acta Metall. Mater. 40 (1992) 205–219.
[40] D.A. Hughes, N. Hansen, High angle boundaries formed by grain subdivision mechanisms, Acta Mater. 45 (1997) 3871–3886.
[41] T. Leffers, R.K. Ray, The brass-type texture and its deviation from the copper-type texture, Prog. Mater. Sci. 54 (2009) 351–396.
[42] R.E. Smallman, D. Green, The dependence of rolling texture on stacking fault energy, Acta Metall. 12 (1964) 145–154.
[43] A.J. Zaddach, C. Niu, C.C. Koch, D.L. Irving, Mechanical properties and stacking fault energies of NiFeCrCoMn high-entropy alloy, JOM (J. Occup. Med.) 65 (2013) 1780–1789.
[44] H. Zhang, Y.Z. He, Y. Pan, S. Guo, Thermally stable laser cladded CoCrCuFeNi high-entropy alloy coating with low stacking fault energy, J. Alloys Compd. 600 (2014) 210–214.
[45] R. Madhavan, R.K. Ray, S. Suwas, Texture transition in cold-rolled nickel–40wt.% cobalt alloy, Acta Mater. 74 (2014) 151–164.
[46] S. Huang, W. Li, S. Lu, F. Tian, J. Shen, E. Holmström, L. Vitos, Scripta Mater. 108 (2015) 44–47.
[47] P.P. Bhattacharjee, S.K. Sinha, A. Upadhyaya, Effect of sintering temperature on grain boundary character distribution in pure nickel, Scripta Mater. 56 (2007) 13–16.
[48] P.P. Bhattacharjee, R.K. Ray, Effect of processing variables on cube texture formation in powder metallurgically prepared Ni and Ni–W alloy tapes for use as substrates for coated conductor applications, Mater. Sci. Eng., A 459 (2007) 309–323.
[49] F.J. Humphreys, M. Hatherly, Recrystallization and Related Annealing Phenomena, second ed.s., Elsevier, Oxford, 2004.
[50] L. Bracke, K. Verbeken, L.A.I. Kestens, Texture generation and implications in TWIP steels, Scripta Mater. 66 (2012) 1007–1011.
[51] L. Bracke, K. Verbeken, L. Kestens, J. Penning, Microstructure and texture evolution during cold rolling and annealing of a high Mn TWIP steel, Acta Mater. 57 (2009) 1512–1524.
[52] A.A. Saleh, E.V. Pereloma, A.A. Gazder, Texture evolution of cold rolled and annealed Fe-24Mn-3Al-2Si-1Ni-0.06C TWIP steel, Mater. Sci. Eng., A 528 (2011) 4537–4549.